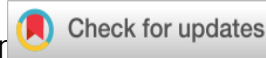
Special section: Geologic, geophysical, and petrophysical interpretation of core data ar



Qualitative and quantitative reservoir bitumen characterization: A core to log correlation methodology

Milad Saidian¹, Torben Rasmussen², Mosab Nasser³, Andres Mantilla⁴, and Rick Tobin⁵

Abstract

Reservoir bitumen is a highly viscous, asphaltene-rich hydrocarbon that can have important effects on reservoir performance. Discriminating between producible oil and reservoir bitumen is critical for recoverable hydrocarbon volume calculations and production planning, yet the lack of resistivity contrast between the two makes it difficult, if not impossible, to make such differentiation using conventional logs. However, the nuclear magnetic resonance (NMR) response in bitumen-rich zones is dominated by short transverse relaxation times (T_2) and a low apparent fluid hydrogen index (HI_{app}) , providing an opportunity to identify the presence of reservoir bitumen. Therefore, NMR logging technology becomes crucial in the characterization of reservoirs in which the presence of bitumen may be of concern. We used NMR and other log data to identify and quantify the occurrence of reservoir bitumen in a carbonate reservoir. A thorough petrophysical evaluation was performed using a full suite of logs, formation pressure measurements, and laboratory core analysis data. We discuss several quick methods to identify intervals with a higher chance of reservoir bitumen presence. The short transverse relaxation times (T_2) and consequently lower T_2 logarithmic mean time values are characteristics of bitumen-rich zones. Another characteristic is low HI_{app} in these zones and consequently lower NMR porosity estimates when compared to porosity estimates from the density and neutron tools. We analyzed 2D longitudinal-transverse relaxation time $(T_1 - T_2)$ maps for core samples at different depths to confirm the presence of reservoir bitumen in some wells using laboratory low-field NMR data. We observed a high T_1/T_2 ratio at various depths, which is an indication of high-molecular-weight hydrocarbons. The presence of bitumen at the same depths was confirmed by thin section analysis, and it is the likely cause for failed formation pressure testing attempts at those depth intervals. Partial cleaning of reservoir bitumen-rich core plugs results in heliuminjection porosity estimates that are too low, and they are closer to the NMR porosity than to density porosity, the latter being more consistent with actual values. In addition, the grain density (GD) calculated by He injection is significantly lower than the GD estimated from elemental capture spectroscopy and X-ray diffraction techniques. Disregarding these effects complicates the core to log correlation, which is common practice for porosity calculations using the density log. A volumetric rock model was used to reconcile core and log data as well as to calculate the saturation of reservoir bitumen. The methodologies for reservoir bitumen characterization introduced here can be applied successfully in different reservoirs for more reliable and precise reservoir evaluation and production planning.

Introduction

The reservoir bitumen formation mechanism is not fully understood. This is reflected in the terminology of high-molecular-weight hydrocarbons (HMWHCs), in which different terms are used to infer different chemical and physical (Dumont et al., 2012) properties or engineering applications. Lomando (1992) lists terminology that is used in the literature to address these hydrocar-

bons: solid hydrocarbon, pyrobitumen, dead oil, black sands, asphaltic sands, tar mats, and solid bitumen. Due to the complex nature of heavy hydrocarbons, Lomando (1992) prefers to use the term reservoir bitumen because it is a descriptive term and avoids confusion with source rock bitumen and kerogen, and it is general enough to cover a wide range of heavy hydrocarbons. There are numerous other definitions and nomenclatures

¹Colorado School of Mines, Department of Petroleum Engineering, Golden, Colorado, USA. E-mail: msaidian@mines.edu.

²Maersk Oil, Houston, Texas, USA. E-mail: torben.rasmussen@maerskoil.com.

³Presently Hess Corporation, Houston, Texas, USA; formerly Maersk Oil, Houston, Texas, USA. E-mail: mnasser@hess.com.

⁴Presently Colombian Petroleum Institute, Piedecuesta, Colombia; formerly Maersk Oil, Houston, Texas, USA. E-mail: andres.mantilla@ecopetrol.com.co.

⁵Presently ConocoPhillips, Houston, Texas, USA; formerly Maersk Oil, Houston, Texas, USA. E-mail: rick.c.tobin@conocophillips.com. Manuscript received by the Editor 17 March 2014; revised manuscript received 14 October 2014; published online 7 January 2015. This paper appears in *Interpretation*, Vol. 3, No. 1 (February 2015); p. SA143–SA158, 14 FIGS., 1 TABLE.

for different heavy hydrocarbons based on properties such as color, reflectance, fluorescence, microsolubility, isotropy, anisotropy, softening point, and density (for more information about these terminologies and their definitions, see Tissot and Welte, 1984, Jacob, 1989, Larsen and Kidena, 2002, Nascimento and Gomes, 2004). In this work, we use the term *reservoir bitumen* as defined by Lomando (1992), and we refer to any hydrocarbon other than reservoir bitumen as *light hydrocarbon*. In the reservoir of interest, there was no indication of gas, and we do not consider gas in this study.

Reservoir bitumen is an immobile hydrocarbon that can have significant effects on the reservoir quality and the production mechanism. When reservoir bitumen is present in significant amounts, identifying the occurrence and quantifying its saturation as well as understanding its distribution in the reservoir are of paramount importance for geologic and engineering modeling and for making economic decisions. Its presence leads to overestimation of reserves, if it is not accounted for. The extent of reduction in porosity and permeability of the rock as a result of precipitation of the reservoir bitumen can be as destructive as the damage caused by carbonate and silica cement (Lomando, 1992). The effect of reservoir bitumen on flow behavior should be investigated in the context of mobility, fluid viscosity, and distribution in the pore space. When HMWHCs are distributed in the pore space and coexist with light and producible hydrocarbons, reservoir bitumen is likely to block pore throats. Conceptually, Dumont et al. (2012) suggest that heavy asphaltene nanoaggregates precipitate on grain surfaces and block some of the pore throats as they segregate in the reservoir by gravity. Precipitated asphaltenes interrupt the migration of the remaining asphaltene aggregates to deeper parts of the reservoir, leading to the formation of asphaltene-rich hydrocarbon patches.

Differentiating reservoir bitumen and light oil using conventional logs such as neutron, density, and resistivity tools is difficult, if not impossible, due to the lack of resistivity and density contrast between light hydrocarbons and bitumen. The use of advanced logging tools such as nuclear magnetic resonance (NMR) and elemental capture spectroscopy (ECS), in conjunction with other logs and core data, allows for differentiation between reservoir bitumen and other hydrocarbon types in the pore space. Nascimento and Gomes (2004) use resistivity logs at different depths of investigation and identify tar-mat-saturated zones by mud invasion profile interpretation. Akkurt et al. (2009) define the missing porosity concept and excessive bound fluid to identify tar-mat-saturated zones using triple combo and NMR logs. *Missing porosity* refers to the portion of porosity not detectable by the NMR logging tool but detectable by other tools such as density and neutron tools. Due to the short relaxation times of the tar mats, the signal from tar and bound water overlaps in the NMR response and results in overestimation of the bound fluid.

In this work, we discuss the effects of the presence of reservoir bitumen on experimental results such as low-field NMR 1D and 2D experiments, helium (He)-injection porosity and grain density (GD), and thin section images. We present a quick-look method using core data, formation pressure data, and log data to qualitatively identify the reservoir bitumen rich zones, and at the same time we use NMR porosity and density porosity log data in a volumetric rock model to quantify the reservoir bitumen saturation in the reservoir. Finally, we present the results of application of the qualitative and the quantitative methodologies in two reservoir bitumen-saturated wells.

Effect of reservoir bitumen on laboratory data Nuclear magnetic resonance porosity

The porosity estimate from NMR is a measure of the number of hydrogen nuclei in a porous medium. Because in a subsurface reservoir system hydrogen is mostly present in water and hydrocarbons, the concentration of hydrogen molecules controls the relationship between the NMR response and fluid volume and ultimately the inferred porosity of the rock. Commonly, the reference fluid for this conversion is freshwater, and the property that defines the concentration of the hydrogen is the $\mathrm{HI}_{\mathrm{app}}$. $\mathrm{HI}_{\mathrm{app}}$ is the ratio of hydrogen nuclei detected by NMR in a known volume of the fluid to hydrogen nuclei detected by NMR in the same volume of water. Although chemically, the HI for viscous hydrocarbons is close to one, HI_{app} can be smaller than one depending on the oil viscosity and NMR acquisition parameters such as echo spacing (LaTorraca et al., 1999). Hence, without correction for low HI_{app} in heavy-oil-saturated and HMWHC-saturated rocks, the NMR derived porosity is underestimated. The presence of gas would also affect NMR porosity because the HI_{app} of the gas is less than one and varies depending on the pressure and temperature condition (for more information, see Akkurt et al., 1996).

Nuclear magnetic resonance T_1 and T_2 distributions

Three relaxation mechanisms control the transverse relaxation (T_2) time for different rock and fluid combinations. These mechanisms, bulk fluid relaxation, surface relaxation, and diffusion relaxation, act in parallel and can be modeled by equation 1 (Coates et al., 1999). Depending on fluid viscosity, chemical composition, rock mineralogy and NMR acquisition parameters, one, two, or all three relaxation mechanisms dominate the relaxation of hydrogen molecules:

$$\frac{1}{T_2} = \frac{1}{T_{2B}} + \frac{1}{T_{2S}} + \frac{1}{T_{2D}},\tag{1}$$

where T_2 is the transverse relaxation time in milliseconds (ms), T_{2B} is the bulk fluid relaxation in ms, T_{2S} is

the surface relaxation in ms, and T_{2D} is the fluid diffusion relaxation in ms.

The fluid diffusion effect is negligible when the NMR response is acquired using short echo spacing (TE) (Carr and Purcell, 1954). The bulk fluid relaxation depends highly on the fluid properties such as viscosity and chemical composition, it varies linearly with temperature, and it can be modeled with equation 2:

$$T_{2B} \cong a \frac{T}{\mu},$$
 (2)

where a is a constant in centipoise (cP)/degrees kelvin (°K)/ms that depends on fluid chemistry, T is the temperature in °K, and μ is the fluid viscosity in cP. Note that equation 2 applies only to the fluids. Bulk relaxation of the gas depends on the pressure and temperature condition.

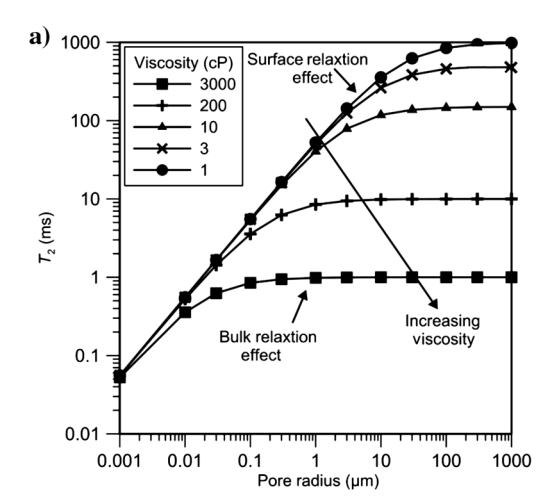
Surface relaxation is dominated by the interactions between fluid and pore surfaces and can be modeled using equation 3 (Coates et al., 1999):

$$\frac{1}{T_{2s}} = \rho_2 \frac{S}{V} = \rho_2 \frac{c}{R},\tag{3}$$

in which ρ_2 is the surface relaxivity ($\mu m/ms$), S is the surface area (μ m²), V is the pore volume (μ m³), R is the pore body radius (μ m), and c is the pore shape constant which is one, two, or three for planar, cylindrical, and spherical pores, respectively (Machado et al., 2011). A similar theory is applied to T_1 distribution except that diffusion relaxation in equation 1 does not exist in T_1 experiments. Also, T_1 is usually significantly higher than T_2 for heavy hydrocarbons. A high T_1/T_2 ratio is characteristic for heavy hydrocarbons and is used to differentiate reservoir bitumen from lighter hydrocarbons. Hirasaki et al. (2003) show that T_1 and T_2 decrease linearly by increasing oil viscosity for samples with viscosity lower than 200 cP. For more viscous samples, T_1 and T_2 reach plateau values and T_1 tend to be higher than T_2 by up to one order of magnitude or more.

We modeled the effect of bulk fluid relaxation and surface relaxivity on the T_2 response for different pore sizes by combining equations 1–3. Figure 1a shows the effect of bulk fluid relaxation time (assuming spherical pores with a constant surface relaxivity of 9 µm/s) on the T_2 response as a function of pore body size. If the pores are saturated with low-viscosity fluid (<3 cP), the effect of pore size on the relaxation time is significant and the time distribution can be considered a representation of the pore sizes for pore radii less than 100 µm. This is due to the fast spin diffusion inside individual pores, which equilibrates the spin density and consequently all the spins in each pore relax with a common relaxation rate (for more information, see Brownstein and Tarr, 1979; Dunn et al., 2002). When pores are saturated with a high-viscosity fluid such as reservoir bitumen (in Figure 1a, viscosity of 3000 cP is modeled), the resulting T_2 is dominated by the bulk fluid relaxation and no effect from the pore size is observed. In such cases, the average T_2 value can be used to estimate the fluid viscosity using empirical correlations (Hirasaki et al., 2003).

Figure 1b shows the effect of surface relaxation on the T_2 response for a different pore body size for a rock sample saturated with a fluid with viscosity of 3000 cP. The surface relaxivity reported in the literature for carbonates is 1–7 μ m/s and for sandstones 6.4–25 μ m/s (Chang et al., 1994; Marschall et al., 1995; Freedman et al., 1997). For pore sizes bigger than 0.3 μ m, changing the surface relaxivity (which can be translated to the mineralogy of the rock) does not have any significant effect on the T_2 time because it is highly dominated by the presence of high-viscosity (short relaxation) reservoir bitumen. Based on the results shown in Figure 1



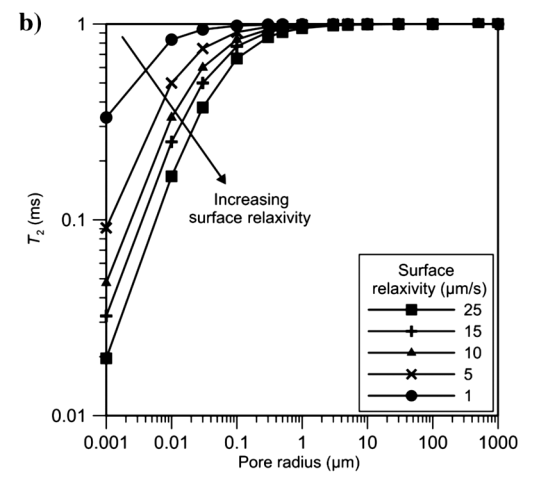


Figure 1. Effect of (a) bulk fluid relaxation time and (b) surface relaxation on the T_2 response (constant surface relaxivity of 9 μ m/s) at each pore body size. In panel (a), the T_2 response is highly dominated by the fluid with very low bulk relaxation (high viscosity). The response is not sensitive to the pore size and will be highly suppressed to shorter relaxation times. (b) When the rock is saturated with a high-viscosity fluid (constant bulk relaxation of 5 ms or approximately 3000 cP) the surface relaxation does not affect the NMR response for pores larger than 0.3 μ m, which shows the dominant effect of fluid bulk relaxation on the response.

in reservoir-bitumen-saturated intervals, the NMR response is dominated by bulk relaxation regardless of the rock mineralogy and it no longer represents the pore-size distribution of the rock. Although reservoir bitumen compromises the conventional application of the NMR logs, its effect on NMR response can be used to identify the reservoir-bitumen-saturated intervals.

In this section, we show how the aforementioned theories about the effect of reservoir bitumen on T_1 and T_2 responses apply in NMR experimental results and interpretation. Figure 2 shows T_1 (dashed line) and T_2 (solid line) distributions for two core samples from different sections of a reservoir at the "native state" and the "cleaned and brine-saturated" conditions. The samples are measured in laboratory conditions using a 2-MHz NMR instrument. Sample 1 (Figure 2a and 2c) is taken from a reservoir-bitumen-saturated interval, and sample 2 (Figure 2b and 2d) is taken from a

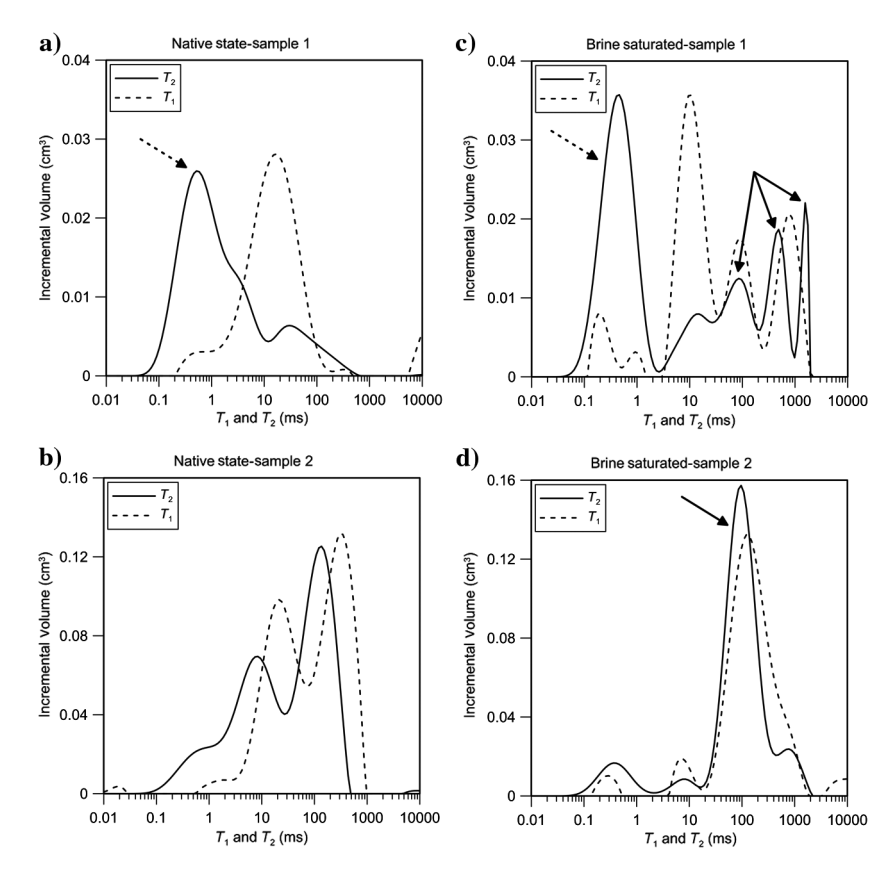


Figure 2. (a and b) T_1 (dashed line) and T_2 (solid line) distributions measured at laboratory condition at native state condition. (c and d) Samples were cleaned by hot solvent extraction, and the measurements were repeated at a brine-saturated condition. Sample 1 is reservoir-bitumen-saturated, and sample 2 is from a water-saturated zone. High T_1/T_2 in sample 1 at the native state is an indication of the presence of reservoir bitumen. This ratio in sample 2 is smaller due to the presence of a lighter phase such as oil-based mud or water. In the brine-saturated condition (c), long relaxing components $(T_1/T_2 \text{ of } 1)$ have been added to the spectrum of sample 1 (solid arrows in panel [c]), but still the T_1 and T_2 distributions are affected due to incomplete extraction and the presence of reservoir bitumen residues (high T_1/T_2). The peaks that correspond to the reservoir bitumen residues are indicated by dashed arrows in panel (c). In sample 2, after extraction, there is no sign of the presence of mud or light hydrocarbon and the T_1 and T_2 distributions are similar.

water-saturated interval. In Figure 2a, the dominant T_1 and T_2 peaks are at 12 and 0.7 ms, respectively. As mentioned earlier, the short T_2 time and high T_1/T_2 ratio in this sample are indications of the presence of heavy hydrocarbons such as reservoir bitumen. Sample 2 (Figure 2b) shows T_1 and T_2 distributions with similar bimodal shapes. A higher average T_2 value (24.4 ms) and a lower T_1/T_2 ratio for the dominant peaks, compared to the same values in Figure 2a, indicate the presence of water and light hydrocarbon such as native oil or synthetic mud. Subsequent to the fresh state measurements, all the samples were cleaned by hot solvent extraction. Then, they were saturated with brine and the same NMR experiments were performed. The NMR responses for both samples (Figure 2c and 2d), show significant differences compared to the response at native state conditions (Figure 2a and 2b, respectively). By cleaning the samples and resaturating with brine,

> new peaks at higher relaxation times appeared in the spectra. The peaks at 300 ms with equal T_1 and T_2 times in Figure 2c and 2d (indicated by solid arrows) are due to replacement of part of the reservoir bitumen with brine. An important observation in Figure 2c is the presence of the peak with a short T_2 and high T_1/T_2 ratio (shown by dashed arrows) after cleaning of the sample. The presence of these peaks suggests that the cleaning process did not remove all of the reservoir bitumen in the pore space. This has been observed in almost all of the core samples taken from the reservoir-bitumen-rich intervals regardless of the volume of the residue in different samples.

Nuclear magnetic resonance T_1 - T_2 maps

Nonuniform pore-size distribution in heterogeneous reservoir rocks and the presence of different fluids with variable viscosity and hydrogen index (HI) make it difficult, if not impossible, to fully characterize the fluids in porous media using just 1D T_1 and T_2 distributions. The T_1 - T_2 correlation maps are used to differentiate the heavy and/or viscous phase from the light phase using the differences in the T_1/T_2 of the fluids (for more information about T_1 - T_2 maps, acquisition, and inversion, see Song et al., 2002). We use this property in T_1 - T_2 correlation 2D maps, to differentiate high- from low-viscosity hydrocarbons. The T_1 - T_2 maps are acquired at the native state for sample 3 (Figure 3a), which is taken from a reservoir-bitumen-saturated interval, and sample 4 (Figure 3b) is taken from a light-oil-saturated interval. The portion of the data that falls on, or close to, the one-to-one correlation line (the black solid line in Figure 3a and 3b) represents light fluids such as light oil, mud, or water in the porous media. Deviation of the data from this line is directly related to the viscosity of the hydrocarbon. The high-amplitude data components, indicated as "heavy HC," for sample 3 (Figure 3a) are due to the presence of reservoir bitumen in this sample. The T_1 - T_2 correlation map for sample 4 (Figure 3b) shows that the sample is saturated with light hydrocarbon and water.

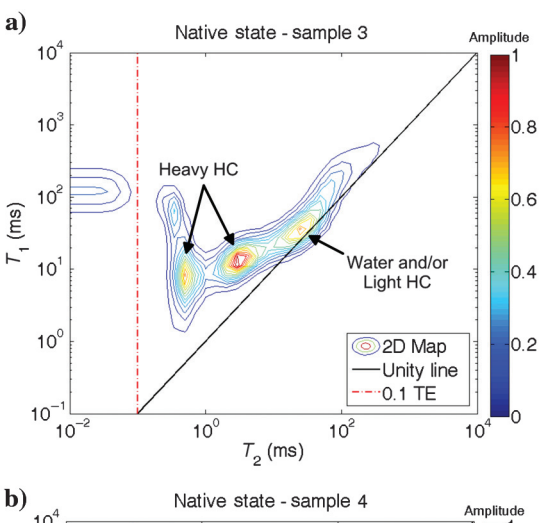
Helium injection porosity

He-injection porosity and air/liquid permeability measurements are common practices in conventional core analysis. Such data are used by petrophysicists for porosity and permeability core to log correlation. Core samples undergo a multistage extraction-cleaning process in the laboratory to clean out oil, mud, and water in the core before the measurements. At the first stage of cleaning, a Dean-Stark extraction-distillation unit was used to extract the water, using toluene for 48 h. The solvent was replaced by chloroform to extract the oil, and then samples were oven dried at 105°C until a constant weight was reached. An attempt was made to remove the heavier components of the oil using higher polarity solvents such as methylene chloride and tetrahydrofuran. As shown earlier in Figure 2a and 2c, despite the multistage cleaning, there are still indications of the presence of reservoir bitumen in the pore space.

Partial cleaning of the samples is due to the insolubility or partial solubility of the HMWHC in polar solvents. Another reason is the blockage of the pore throats by the reservoir bitumen, which prevents the solvent from reaching parts of the pore space (Wilhelms et al., 1994). In both cases, using high-polarity solvents and increasing the cleaning time would increase the efficiency of the cleaning process. Figure 4a shows the core He porosity and density log evaluated total porosity data for samples that are taken from a well that has no indication of reservoir bitumen presence (henceforth, we refer to this as Well 1). The density log total porosity is calculated without consideration of the possibility of bitumen in the pore space. A more thorough discussion of how to incorporate the bitumen in the density log total porosity evaluation will be presented later.

The porosity values from density and He injection are in good agreement for Well 1. We performed the same comparison for a set of samples taken from a well and its side track that are affected by the presence of reservoir bitumen (henceforth, we refer to this well and its side track as Wells 2 and 2ST, respectively). The results are shown in Figure 4b, in which core He porosity is systematically lower than the log density total porosity. This is due to the presence of reservoir bitumen residue in the cores even after two-stage extraction. As mentioned earlier, similar to He porosity, NMR log porosity calibrated with freshwater shows lower porosity

than density derived total porosity. The NMR log porosity (calibrated using HI of 1 for water) and He-injection porosity data for Well 2 and its side track are shown in Figure 5. Although both porosity values underestimate the rock porosity compared to density log total porosity, they show better agreement than in Figure 4b. This comparison shows a common source of error, which is the presence of reservoir bitumen, for NMR log and Heinjection measurements. The possibility of pore throat blockage by reservoir bitumen due to partial sample cleaning discussed above could cause an additional porosity deficit when He-injection porosity values are compared to NMR porosity values. However, only an unknown fraction of the reservoir bitumen in the pore space is spatially configured to result in isolated pockets of pore space undetectable by the He-injection



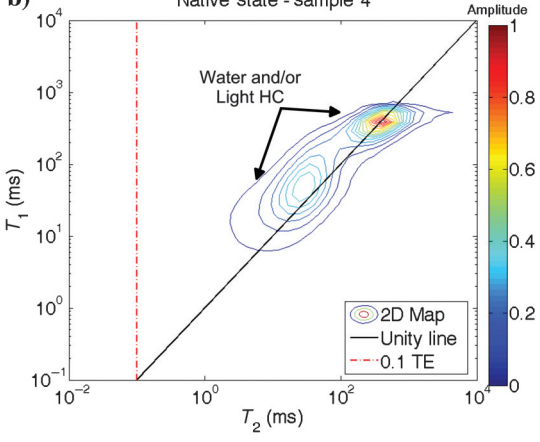
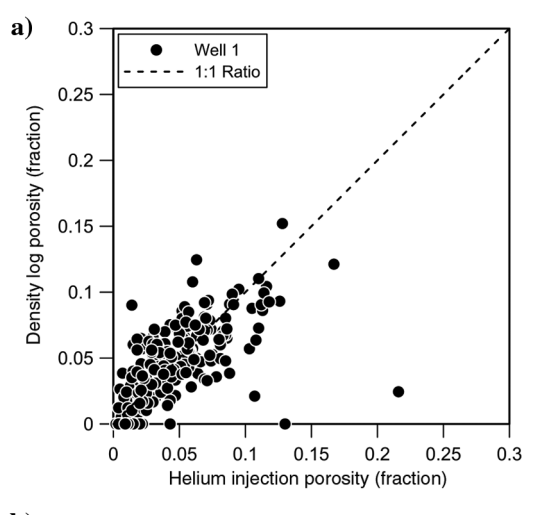


Figure 3. Note the T_1 - T_2 correlation maps for (a) a reservoir-bitumen-saturated sample and (b) a light-fluid-saturated sample. The red dashed-dotted line is the minimum relaxation time measurable with the NMR instrument, which is 100 μ s. Any data point on the left side of this line is either noise or a mathematical inversion artifact. The black solid line is the 1:1 ratio line, and the color bar is the normalized signal intensity. The presence of data components with a short T_2 and a very high T_1/T_2 ratio in panel (a) indicates the presence of reservoir bitumen in the sample. All of the components on the 1:1 ratio lines in panels (a and b) correspond to light hydrocarbon and/or water responses.

measurement. On the other hand, the cleaning procedure before the He-injection measurement might result in removal of an unknown amount of reservoir bitumen, thus increasing the He-injection porosity compared to NMR log porosity. It is likely that some of the scatter seen in Figure 5 is related to these opposite effects, which we consider relatively small but have not been able to quantify.

Grain density measurement

GD measurement using He injection is a reliable way to calibrate the GD measured by the ECS log and calculate the total porosity using density logs (Wilhelms et al., 1994). Evaluating the total porosity using constant mineralogy and fluid type often results in poor estimation of porosity, especially in heterogeneous systems (Elseth et al., 2001). The presence of low-density (compared to mineral densities) reservoir bitumen residue in the pore space due to partial cleaning reduces the He-



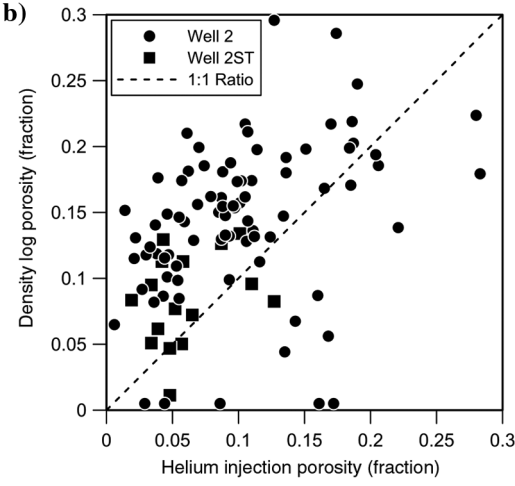


Figure 4. Density porosity and He porosity crossplot (a) light-oil-saturated well (Well 1) and (b) reservoir-bitumensaturated well (Well 2) and its side track well (Well 2ST). Both porosity values are in good agreement in panel (a), but He injection systematically underestimates the porosity values in panel (b).

injection GD (Wilhelms et al., 1994) because during the measurement, the bitumen is part of the solid matrix rather than a saturating fluid.

Another method to determine the GD is using X-ray diffraction (XRD) data. This method quantifies the mineralogy of the rock based on the angle of diffraction of the scattered X-ray beam, after collision with the crystalline structure of the mineral. A decrease in the crystal size or a lack of crystallinity will reduce the intensity of the diffracted beam (for more information, see Ruessink and Harville, 1992). Thus, XRD results are not affected by the reservoir bitumen regardless of the saturation due to the noncrystalline structure. Note that XRD is not a direct GD measurement technique, and in this study, we use the mineral constituents of the rock determined by XRD and GD values for pure individual minerals to calculate the GD using the following equation:

$$\rho_g = \frac{100}{\sum (\text{wt}\%_{\text{min}}/\rho_{\text{min}})},\tag{4}$$

where ρ_g is the GD of the rock sample in gr/cm³, wt%_{min} is the weight percent fraction of each mineral, and ρ_{min} is the density of the pure mineral in gr/cm³.

Figure 6 shows a comparison between GD evaluated by XRD and He porosity measurements. In Well 1 (Figure 6a), the XRD and He-injection GD results in similar values. In Wells 2 and 2ST (Figure 6b), the XRD GD is higher, and it shows no correlation with the calculated GD by He injection. In Wells 2 and 2ST, the presence of varying amounts of low-density reservoir bitumen residue has affected the GD whereas the XRD method only considers the hydrocarbon-free GD. Using He-injection

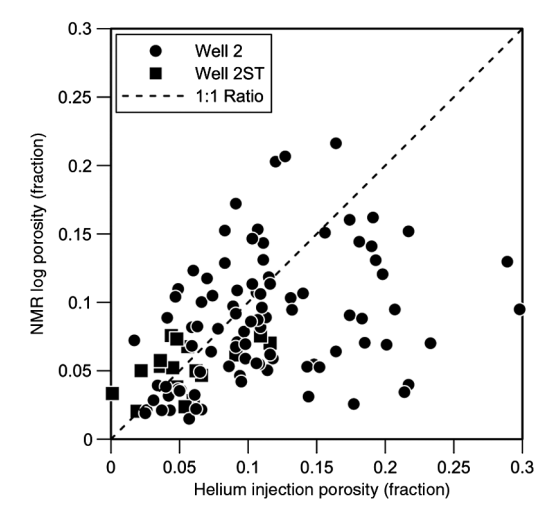


Figure 5. Crossplot of NMR log porosity and He-injection porosity values for reservoir bitumen-saturated well and its side track well (Wells 2 and 2ST, respectively). NMR log and He-injection porosities are affected by presence of reservoir bitumen in the pore space. Due to the underestimation of the porosity in both measurements, He-injection porosities are in better agreement with NMR porosity than with density porosity values.

GD values for core-log correlation without considering the effect of reservoir bitumen residue results in underestimation of the total calculated using the density log. There are other sources of GD estimates such as ECS logs and multimineral analysis, which theoretically are reservoir-bitumen-independent and can be used for core-to-log correlation of the GD for a more precise density porosity calculation. Figure 7 shows a schematic of which parts of the reservoir rock are detected by different log and core laboratory measurement techniques.

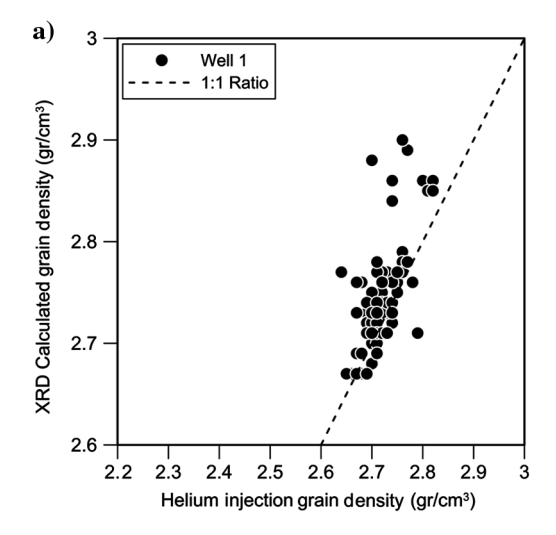
Petrographic analysis

Petrographic analysis of thin sections can be used to detect the presence of reservoir bitumen in reservoir rocks. It can provide direct confirmation of the presence of reservoir bitumen in reservoirs. In a thin section, reservoir bitumen is recognized as a solid cement that occurs in a variety of geometries, including meniscus pore wall coatings (Figure 8a and 8b), solidified droplet shapes, pore-bridging ribbons (Figure 8c and 8d), and as complete or nearly complete pore-filling material (Figure 8e). Reservoir bitumen is opaque in transmitted plane light or cross-polarized light, and it is blackishbrown to black in reflected light. Desiccation cracks may appear within the bitumen fill (Figure 8e) originating from either natural shrinkage or laboratory-induced desiccation resulting from the cleaning and drying process. In ultraviolet light, bitumen will appear black, nonreflective, and will not show any sign of fluorescence. An example of a clean, nonbitumen-saturated thin section is shown in Figure 8f.

Reservoir bitumen is difficult to confuse with other types of solid opaque cements such as pyrite or iron oxides. Pyrite does not occur in meniscus, droplet, ribbonshaped, or pore wall coating morphologies, and in reflected light it will exhibit a characteristic gold color. Also, iron oxides are readily distinguished from bitumen by their characteristic rust to red colors in reflected light.

To preserve bitumen for petrographic observation, the core plugs used to make thin sections should be cleaned enough to remove brine, movable (liquid) oil, and drilling mud, but not so aggressively cleaned that the solid components are removed. If thin sections are made from the core plug end trims, the cleaning procedure used should match the protocol used for routine core analysis so that the visual evidence observed in thin sections matches the core analysis data results quantitatively. The protocol used can vary depending on the desired results. Three levels of cleaning may be used: (1) nonaggressive cleaning to remove brine and drilling mud while preserving all of the oil components (volatile liquid oil stain and solid bitumen). In thin section, an oil stain will appear as a thin brown coating that may fluoresce in ultraviolet light, and the solid bitumen will be opaque, black and nonfluorescent; (2) additional solvent cleaning to remove the volatile liquid stain, leaving behind only the solid bitumen in the pores. This will yield a thin-section view with porosity estimates that should reasonably match core analysis results as well as downhole NMR porosity calculations; and (3) highly aggressive, longer duration cleaning (especially at high temperatures) to remove all hydrocarbon components. This method yields a clean, open-pore system showing no evidence of hydrocarbon migration. Thin-section estimates of porosity in this case may match uncorrected, uncalibrated density log estimates, but they will not likely match NMR log results. However, the thin-section porosity values can be used to estimate the total potential porosity elsewhere where solid bitumen might be absent.

Petrographic work can be integrated into the bitumen assessment process described in this study in three



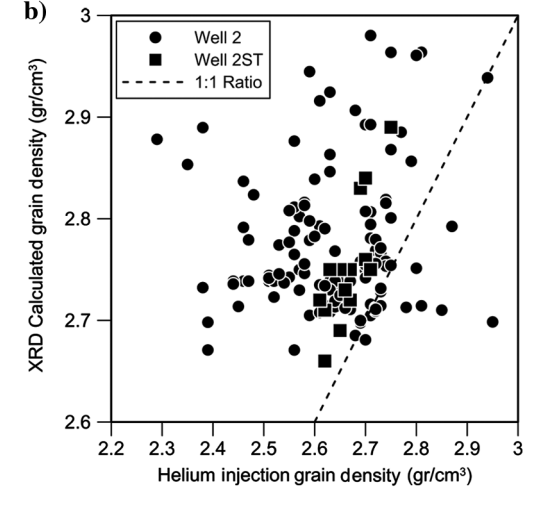


Figure 6. Crossplot of GD calculated by He-injection and XRD data for the (a) light-oil-saturated well (Well 1) and (b) reservoir bitumen-saturated well and its side track (Wells 2 and 2ST, respectively). In Well 1 (a), the XRD and He-injection GD result in similar values, whereas in Wells 2 and 2ST (b), the XRD GD (not affected by HC remnants) is systematically higher than the calculated GD by He-injection data (which are affected by the HC residues). Using He-injection GD values for core-log correlation without considering the effect of reservoir bitumen residue results in underestimation of the porosity calculated using density log.

basic ways: (1) qualitative visual confirmation of downhole log results, (2) quantitative measurement of volume percent solid bitumen, volume percent pore space, volume percent solid minerals, and (3) determination of relative and/or absolute oil charge timing. Relative timing may include timing versus other diagenetic burial events, and it may include initial charge, recharge, flushing, and biodegradation events. Absolute geologic timing may be interpreted for single or multiple events, and it may include information about temperature, pressure, and depth conditions that existed in the reservoir strata. In this study, we use the petrographic analysis of the thin sections for qualitative visual confirmation of the presence of the reservoir bitumen.

Reservoir bitumen quick identification method

As discussed earlier, the presence of reservoir bitumen in the rock has a significant effect on the laboratory and downhole NMR responses as well as laboratory tests such as thin sections, porosity, and GD measurements. Any of these indicators taken individually might not be sufficient to positively identify reservoir bitumen, but taken together, the agreement of all or some of these indicators provides a stronger indication of the presence of reservoir bitumen. We used these effects to develop a quick identification method to differentiate the reservoir-bitumen-saturated and light-fluid-saturated intervals. The following list describes the stepwise workflow for reservoir bitumen identification.

Step 1: T2 distribution

For a proper interpretation of the T_2 distributions, fluid saturations and viscosities are required. Equation 1 provides a correlation to calculate the approximate

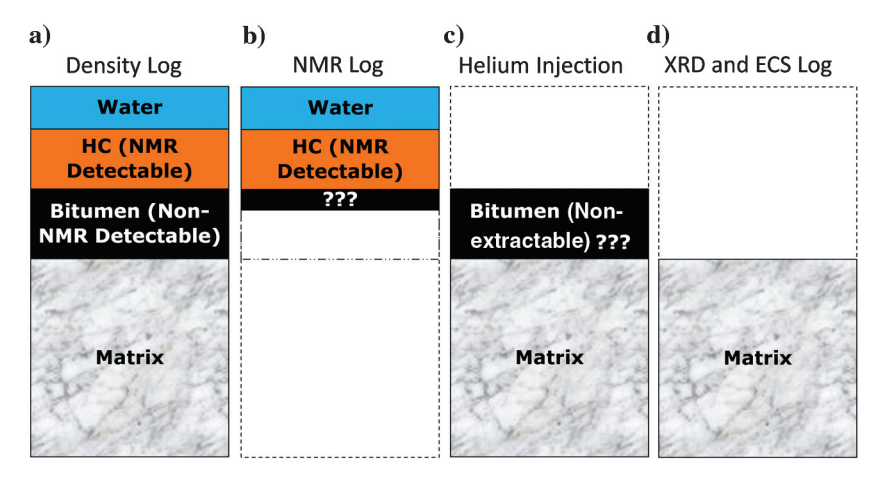


Figure 7. Volumetric rock model that shows the portion of the rock and fluid for different measurements. (a) Density log measures the bulk density of the rock including all the minerals and the fluids in the pore space. (b) NMR porosity includes the light fluids and part of the heavy hydrocarbons such as reservoir bitumen indicated by "???" in the figure. (c) He-injection calculated GD includes the rock matrix and the hydrocarbon remnants, which are the results of incomplete extraction. (d) XRD and ECS logs measure the weight fraction of each mineral constituent in the matrix. By assuming a density value for each individual mineral, the GD can be calculated.

bulk relaxation for oils using viscosity and reservoir temperature.

As described earlier (Figure 1), in reservoir bitumensaturated intervals, the short bulk T_2 relaxation of the bitumen dominates the T_2 spectrum Therefore, visual inspection of the T_2 distribution enables a first assessment of the fluid type.

Step 2: Density (total)-nuclear magnetic resonance porosity

Presence of low-HI_{app} fluids, such as high-viscosity hydrocarbons or gases, reduces the estimated porosity from the NMR tool. Plotting the density porosity and NMR porosity on the same scale helps us identify the zones in which NMR shows a deficit in porosity. Due to uncertainties associated with GD and liquid phases especially in high-clay-content, heterogeneous, and thinly layered reservoirs, it is challenging to define a universal threshold for NMR-density porosity difference as an indication of presence of reservoir bitumen. Precise depth matching in reservoirs with rapidly variable porosity with depth is crucial prior to density-NMR porosity comparison. A slight mismatch could result in a significant porosity deficit and misinterpretation of an interval as reservoir bitumen rich.

Step 3: Density (total) porosity- T_{2LM} crossover

For light-hydrocarbon-saturated or water-saturated rocks (assuming $\mathrm{HI_{app}}$ of 1 for both fluids), the T_2 distribution can be considered as a representation of the pore-size distribution and the T_2 logarithmic mean (T_{2LM}), calculated by equation 5, will be an indication of the pore size that dominates the porosity of the rock:

$$T_{2\text{LM}} = \exp\left(\frac{\sum \ln(T_{2i}) \times \phi_i}{\sum \phi_i}\right), \quad (5)$$

in which T_{2LM} is the logarithmic mean of the T_2 distribution measured in ms. If the T_2 distribution spectrum is plotted using i number of points (bins), the ith bin has a T_2 time (T_{2i}) and an amplitude that is the porosity associated with that bin (ϕ_i).

The $T_{\rm 2LM}$ and density porosity crossover is an indicator of whether the T_2 response is dominated by rock or fluid properties. In clay-free intervals saturated with light oil and water, we expect to see an increase in $T_{\rm 2LM}$ as a result of increase in porosity. Presence of reservoir bitumen shifts the T_2 distribution toward shorter relaxation times, and consequently $T_{\rm 2LM}$ decreases significantly and does not follow the porosity variation. Density porosity, regardless of the bitumen content, captures the variations in porosity. Fluid and rock effects on T_2 distribution can be separated by plotting

density porosity and $T_{\rm 2LM}$ on the same track. They should be scaled so that they approximately overlap in water-saturated or light-hydrocarbon-saturated intervals (for example, 30 to 0 p.u. for porosity and 0 to 700 ms on the linear scale for $T_{\rm 2LM}$).

Step 4: Grain density comparison

Plotting different GD data sets on the same track helps to confirm the presence of reservoir bitumen in the intervals that have low He-injection calculated grain densities, compared to other measurements such as XRD, ECS, or multimineral analysis.

Step 5: Petrographic screening

Available thin sections were used to visually confirm the presence of solid pore-filling bitumen. We created a log in which we assigned a value of one for petrographic images that show the presence of bitumen (Figure 8a–8e) and a value of zero for reservoir bitumen free images (Figure 8f).

Step 6: Downhole pressure test

Downhole formation pressure tests are used to measure the fluid mobility at different depths. Taken independently, formation pressure tests are not an indication of the presence of reservoir bitumen. A dry or failed pressure test can be either due to low permeability of the rock or high viscosity of the fluid. In this study, we assigned zero to the failed or dry pressure tests and one to the tests that recorded a pressure build up.

Reservoir bitumen quantification: Volumetric model

In the previous section, a stepwise quick, but qualitative, identification method for reservoir bitumen was presented. In this section, we discuss a volumetric model to quantify the saturation of the reservoir bitumen and refine the total porosity estimation for hydrocarbon volume calculation purposes.

Figure 9 shows a schematic of the reservoir rock model developed. The question mark in Figure 9 indicates that the cleaning process in the core laboratory will remove an unknown amount of the reservoir bitumen present in the reservoir. It is assumed that this portion of the hydrocarbon is undetectable by the NMR logging tool in the reservoir. The amount of removed bitumen is expected to be small; therefore, the matrix density values reported from He-injection core

analysis ($\rho_{\rm macore}$) will be smaller than the matrix density of the reservoir rock ($\rho_{\rm ma}$). Likewise, the bitumen in the reservoir is nonmovable, so it is effectively part of the rock, and the log-derived apparent reservoir matrix density ($\rho_{\rm mares}$), is close to $\rho_{\rm macore}$, as detailed later. The limestone reservoirs under consideration here are essentially shale free, and there was no shale included in the model.

Total porosity calculated from the density log using a standard matrix density will include the part of the pore space occupied by bitumen. The total porosity value including the volume of bitumen $(\phi_{\rm max})$ is larger than the core analysis derived value and the total porosity value from an NMR log, which does not detect the bitumen (Figure 7).

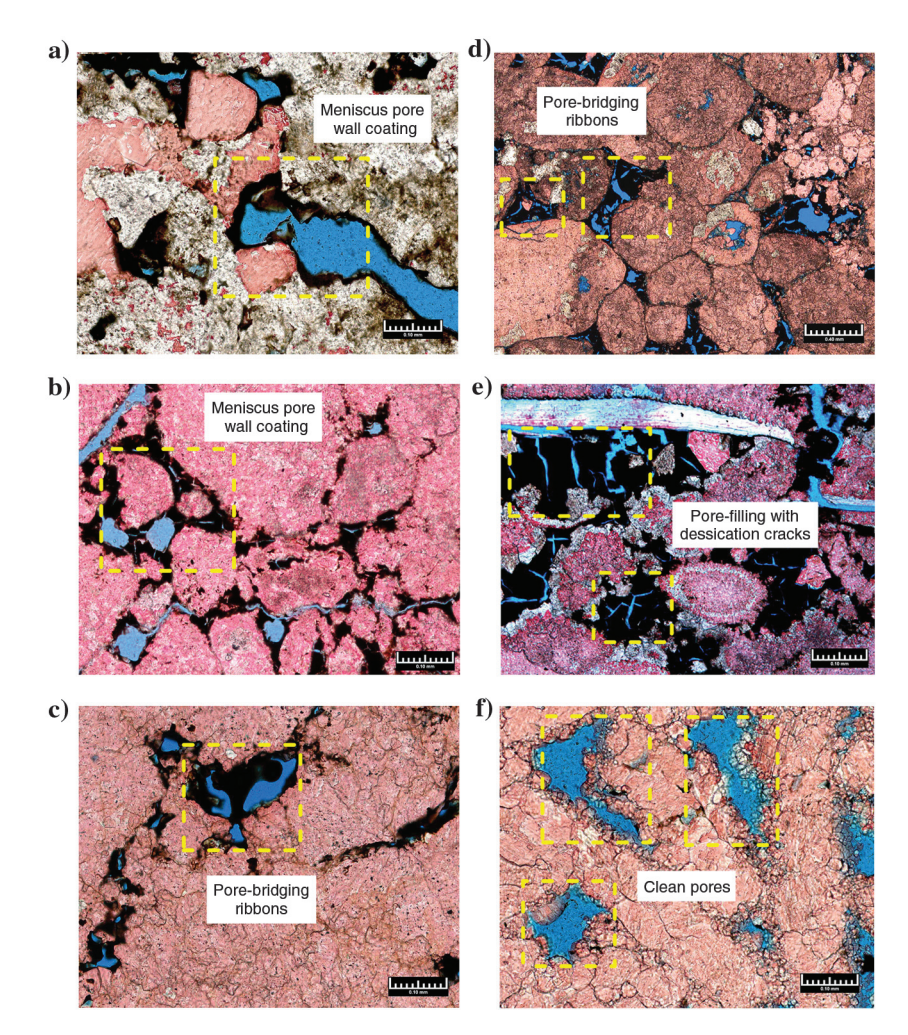


Figure 8. In thin sections, reservoir bitumen is recognized as a solid cement that occurs in a variety of geometries, including (a) pore-lining, meniscus bitumen in dolomite reservoir facies, (b) meniscus bitumen pore linings in limestone, (c) pore-lining bitumen and pore-bridging ribbon of bitumen in limestone facies, (d) pore-lining and pore-bridging bitumen in oncoidal limestone facies, and (e) pore-filling bitumen with dessication cracks in a skeletal limestone. Examples of each bitumen geometry are annotated and shown using dashed boxes. In all cases, reservoir bitumen has reduced the pore volume and decreased the permeability by restricting pore throats. Panel (f) shows a limestone sample that is not damaged by the presence of reservoir bitumen. The blue color in all images is the epoxy that has been used for thin-section preparation.

The effect of the presence of reservoir bitumen on the evaluation of porosity can be quite significant. Consider a reservoir with matrix density $\rho_{\rm ma}=2.75~{\rm gr/cm^3}$ with two different porosity values, $\phi_{\rm max}=0.25~{\rm and}$ $\phi_{\rm max}=0.10~{\rm and}$ varying amount of reservoir bitumen. The water saturation (S_{wt}) in the two situations is 20% and 40%, respectively. If the total porosity is calculated from the density log without acknowledging the presence of varying amounts of reservoir bitumen, the total porosity will be significantly higher than the NMR porosity, even for moderate amounts of reservoir bitumen (Figure 10). This suggests that the combination of the total porosity estimation from the density log and the NMR porosity can be used to quantify the amount of reservoir bitumen.

Figure 10a and 10b shows the effect on porosity estimates of varying amounts of reservoir bitumen in the pore space in the two examples, respectively. It is interesting to note that for bitumen saturations larger than, e.g., 20%, the difference between the evaluated total porosity and the NMR porosity becomes significant (>15%). The *effective* reservoir matrix density (ρ_{mares}), which decreases rapidly with increasing bitumen saturation, can be derived from the model equations presented below to be compared to the core analysis matrix density (ρ_{macore}) values, which should also include the reservoir bitumen assuming it has not been removed in the core cleaning process.

When logging the reservoir, it is assumed that the NMR tool and the density tool (measuring ρ_B) respond to the same fluid in the pore space due to their similar measurement depths of investigation; i.e., the relevant water saturation for the model is S_{xo} . We will denote the saturation of NMR-detectable hydrocarbon and non-NMR-detectable hydrocarbon as $S_{\rm HC}$ and $S_{\rm RB}$, respectively. All saturations are with reference to $\phi_{\rm max}$, which is the porosity of all the nonmineral portions of the rock (Figure 9). With the model and nomenclature given in Figure 9, the following relationships can be derived:

$$\rho_{\rm fl}\phi_{\rm fl} = S_{\rm xo}\phi_{\rm max}\rho_W + (\phi_{\rm fl} - S_{\rm xo}\phi_{\rm max})\rho_{\rm HC},\tag{6}$$

Reservoir rock model

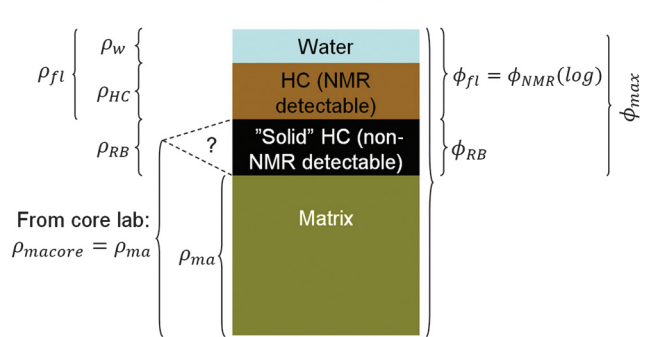
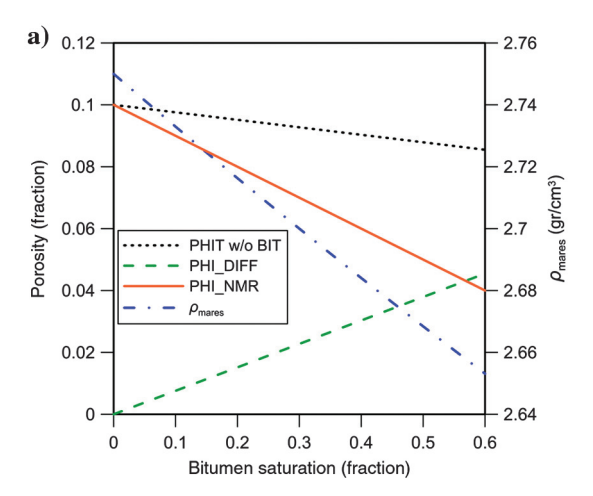


Figure 9. Reservoir rock model annotated with relevant density and porosity labels used in the text. The question mark indicates that the cleaning process will remove an undefined amount of the reservoir bitumen, which is itself undetectable by the NMR logging tool in the reservoir.

$$\rho_B = \rho_{\rm fl} \phi_{\rm fl} + \rho_{\rm RB} \phi_{\rm RB} + \rho_{\rm ma} (1 - \phi_{\rm fl} - \phi_{\rm RB}), \tag{7}$$

where $\rho_{\rm fl}$ and $\phi_{\rm fl}$ are the density and porosity of the fluids that are detectable by NMR, respectively, and $\rho_{\rm W}$ and $\rho_{\rm HC}$ are the densities of water and light hydrocarbons in the rock, respectively. Assuming $\phi_{\rm fl} = \phi_{\rm NMR}$ (the logged NMR porosity in Figure 9), we can rearrange equations 6 and 7 for $\rho_{\rm fl}$ and $\phi_{\rm RB}$, which is the reservoir bitumen porosity, and eventually calculate $S_{\rm RB}$, which is the reservoir bitumen saturation:



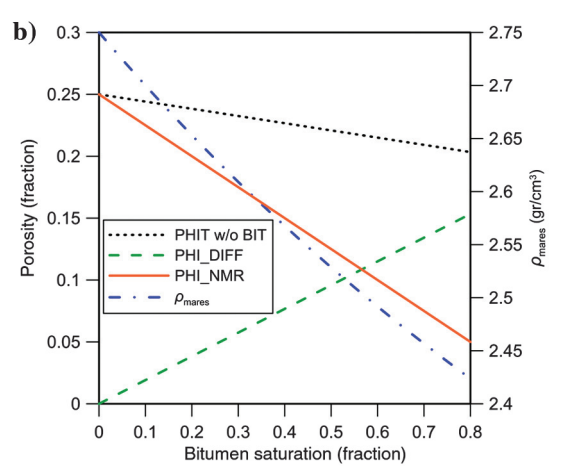


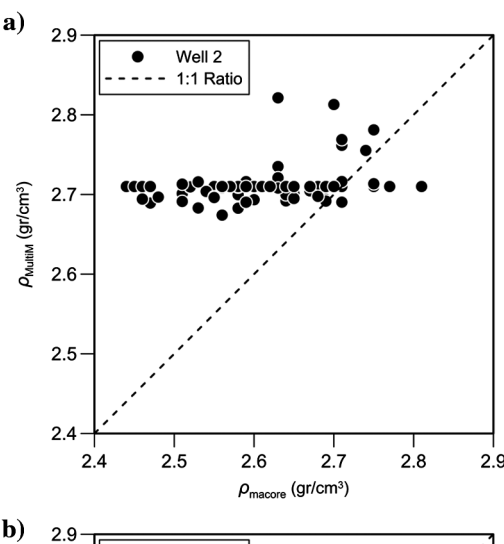
Figure 10. Effect on porosity estimates of varying amounts of bitumen in the pore space in two examples: (a) PHI_MAX = $0.10 \text{ and Swt} = 0.40 \text{ and (b) PHI_MAX} = 0.25 \text{ and Swt} = 0.20.$ The black dotted lines indicate the total porosity evaluated without consideration of the presence of the reservoir bitumen, i.e., considering all hydrocarbon (oil and reservoir bitumen) as oil for oil density calculation. The solid brown lines are the porosity that can be detected by an NMR tool, which cannot detect the "solid" reservoir bitumen. The dashed-dotted blue lines indicate the reservoir matrix density (ρ_{mares}), i.e., the combined density to the mineral volume and the varying amount of reservoir bitumen. The dashed green lines are the difference between total porosity and NMR porosity. For bitumen saturations larger than 20%, the difference between the evaluated total porosity and the NMR porosity becomes significant (>15%). The reservoir matrix density ($\rho_{\rm mares}$) decreases rapidly with increasing bitumen saturation.

$$\rho_{\rm fl} = \frac{S_{\rm xo}\phi_{\rm max}\rho_W + (\phi_{\rm NMR} - S_{\rm xo}\phi_{\rm max})\rho_{\rm HC}}{\phi_{\rm NMR}}, \qquad (8)$$

$$\phi_{\rm RB} = \frac{\rho_{\rm B} - \phi_{\rm NMR} \rho_{\rm fl} - \rho_{\rm ma} (1 - \phi_{\rm NMR})}{\rho_{\rm RB} - \rho_{\rm ma}} = \phi_{\rm max} - \phi_{\rm NMR}, \eqno(9)$$

$$S_{\rm RB} = \frac{\phi_{\rm RB}}{\phi_{\rm max}}.$$
 (10)

To solve for the bitumen content, an iterative approach is used. First, the total porosity (ϕ_t) from the density log is calculated following an iterating approach using density porosity log data and Archie's equation (or any appropriate water saturation model) using an initial guess for $\rho_{\rm flt}$ until stable values of ϕ_t , water saturation (including S_{xo}), and total fluid density ($\rho_{\rm flt}$ in equation 11) are obtained. In the first calculation, there is no attempt to include the effect of bitumen. In the



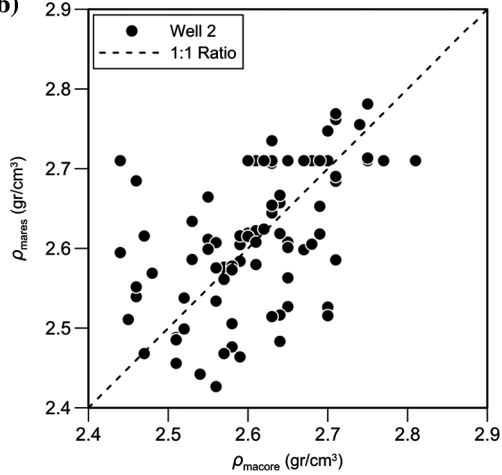


Figure 11. Well 2 core analysis matrix density (ρ_{macore}) plotted against two log-based matrix density estimates: (a) using a multimineral-based log estimate of matrix density not including the effect of bitumen and (b) using the approach given here including the effect of reservoir bitumen.

presence of bitumen the initial calculated value of ϕ_t will be too small (compared to $\phi_{\rm max}$) as bitumen is denser than the movable oil and the bitumen will be treated as movable oil. The next step is to calculate equations 8–10 above using ϕ_t for $\phi_{\rm max}$. The total porosity calculation is now repeated with the modification that the fluid density $\rho_{\rm flt}$ is calculated using $S_{\rm RB}$ and the associated $\rho_{\rm RB}$ in the following manner:

$$\rho_{\text{flt}} = S_{\text{xo}} \rho_{\text{W}} + (1 - S_{\text{xo}} - S_{\text{RB}}) \rho_{\text{HC}} + S_{\text{RB}} \rho_{\text{RB}}. \tag{11}$$

The total porosity ϕ_t and $S_{\rm xo}$ are then fed into equations 8–10, and the process is repeated.

In addition to the standard log evaluation, the above procedure results in an estimate of $S_{\rm RB}$. Here, we use $S_{\rm RB}$ as a bitumen indicator for values larger than 0.25. Note that $S_{\rm RB}$ can also be used to calculate the fraction of pore space of the reservoir that is occupied by bitumen and as a guide to the distribution of the bitumen.

It is possible to derive an estimate of the apparent reservoir matrix density ($\rho_{\rm mares}$), i.e., including the bitumen as

$$\rho_{\text{mares}} = \frac{\phi_{\text{RB}}\rho_{\text{RB}} + (1 - \phi_{\text{NMR}} - \phi_{\text{RB}})\rho_{\text{ma}}}{1 - \phi_{\text{NMR}}}$$
$$= \frac{\rho_{B} - \rho_{\text{fl}}\phi_{\text{NMR}}}{1 - \phi_{\text{NMR}}}.$$
 (12)

The apparent reservoir matrix density (ρ_{mares}) should compare favorably to the He-injection derived matrix density (ρ_{macore}) values, which also include the effect of bitumen.

Figure 11 illustrates the robustness of the method. Figure 11a is a crossplot of core analysis matrix density (ρ_{macore}) for whole core and plug samples from Well 2 plotted against the result of a multimineral model (ρ_{MultiM}) , which includes quartz, calcite, and dolomite. In Figure 11b, the same core data (ρ_{macore}) are plotted against the calculated ρ_{mares} using the method described above. The match is not perfect, but the trend is clear, and the method properly includes apparent matrix density values as low as 2.45 g/cc.

As discussed above, density derived values for total porosity will be smaller than the "true" total porosity of the model, $\phi_{\rm max}$ (Figure 9), if the bitumen is not properly included in the fluid density that enters the total porosity calculation. This is because the bitumen is treated as belonging to the fluid in the pore space. Incorporating the bitumen will actually increase the evaluated total porosity as compared to a standard evaluation, not accounting for bitumen, and make the agreement with core derived values even poorer. The NMR porosity, on the other hand, should be in much better agreement with the core derived values as the NMR log does not respond to the bitumen part, which in this context can be considered solid (Figure 5). Figure 12

illustrates the increase in total porosity from the density log when bitumen is included (PHIT) as compared to not included (PHIT_NO_RB_EFFECT) in the evaluation of a bitumen-rich section of Well 2. It can be seen that including the effect of bitumen can increase the evaluated total porosity significantly.

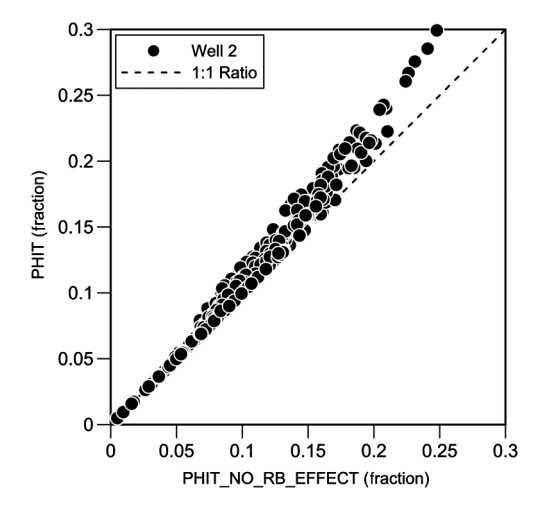


Figure 12. Illustration of the effect of including the bitumen in the total porosity (PHIT) calculation as opposed to not including bitumen in the calculation (PHIT_NO_SHC_EFFECT) for Well 2. It can be seen that including the effect of bitumen can increase the evaluated total porosity significantly.

Case study and discussion

The explained methodologies for quick identification and volumetric modeling was applied to two wells with reservoir bitumen-saturated intervals. The reservoir under consideration was presalt Cretaceous carbonate, more specifically an Aptian lacustrine microbial limestone, located in the deep water Campos basin off shore Brazil. Several wells with varying amounts of reservoir bitumen have been drilled in the area. In this paper, we only discuss wells with high levels of reservoir bitumen. The wells were drilled with oil base mud and were logged with wireline standard triple combo suites, NMR, ECS, and formation pressure tests. The logging operations were carried out successfully and the data quality is good for all reservoir sections discussed here.

The log tracks for Wells 2 and 3 are shown in Figures 13 and 14, respectively. Details of each log track are given in Table 1. In Well 2 (Figure 13), three zones have been observed. At the top and bottom, there are two low-resistivity water-saturated intervals (zones C and A, respectively). Zone B in Figure 13 with low gamma ray (GR), high resistivity (RSHAL and RT), and high-density porosity (PHIT) is shown. The resistivity, density, and neutron logs at this interval show all the characteristics of a prolific oil-saturated reservoir. This is similarly observed in the top interval (zone B) of Well 3 shown in Figure 14.

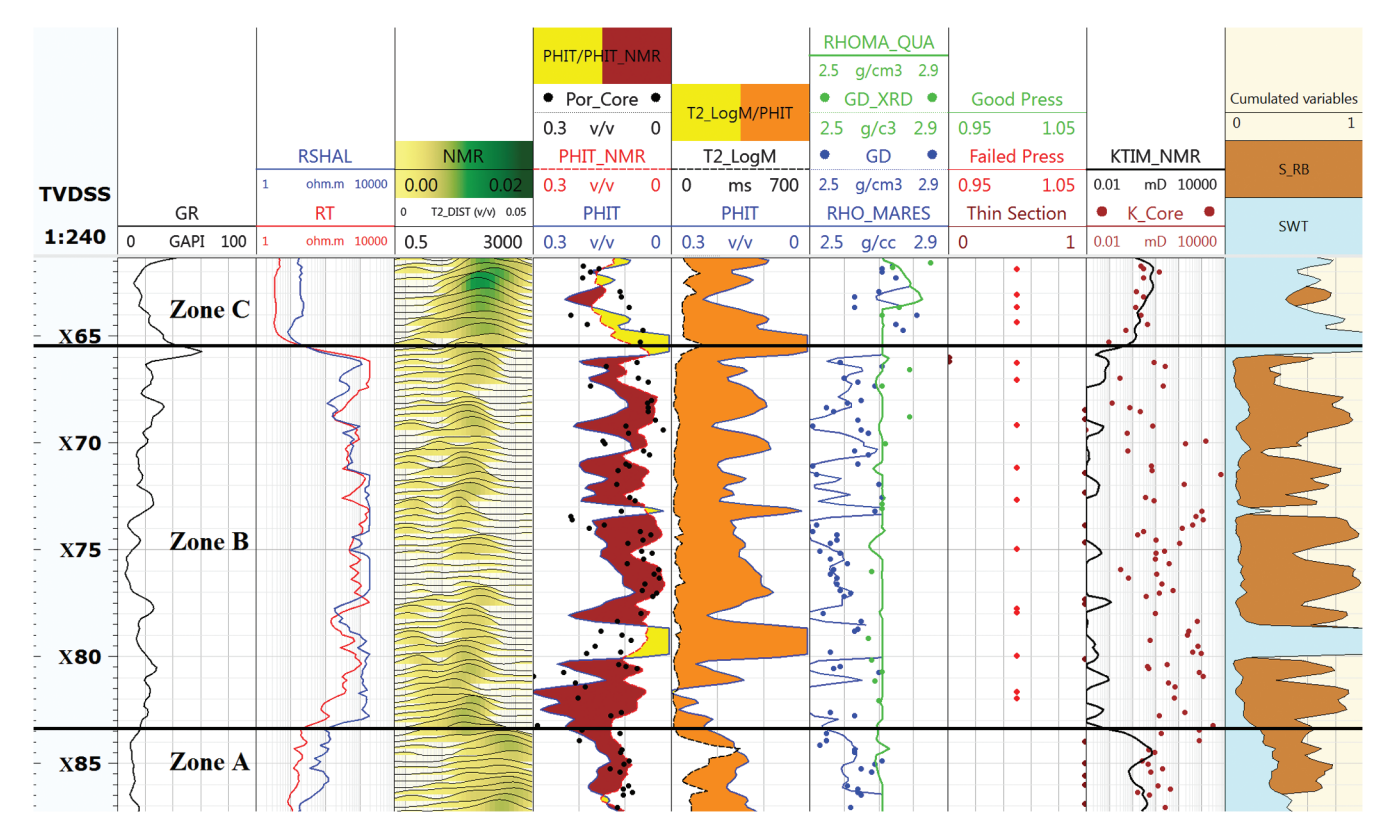


Figure 13. Log and core data for Well 2. Log track details are given in Table 1. The well shows three zones: Zone A is a mixed water-/oil-/bitumen-saturated zone, zone B is a bitumen-saturated zone, and zone C is water saturated. Quick identification steps are shown in different log tracks. A detailed discussion for each track is given in the "Case study and discussion" section.

We followed the stepwise quick identification for both wells to differentiate reservoir bitumen-saturated intervals. In the following, after discussing each log track, the corresponding quick identification step will be addressed.

Track 4 in both wells shows the changes in NMR T_2 distribution (T2_DIST) when the NMR logging tool enters zones B of both wells. We observed that the presence of heavy hydrocarbon dominates the NMR response and shifts the distribution toward faster relaxation times (step 1).

The brown fill in track 5 indicates the areas that NMR porosity (PHIT_NMR) is underestimating the porosity in comparison to the density porosity (PHIT) He-injection porosity data (Por_Core) is also shown. As shown earlier in Figure 5, they are closer to NMR porosity due to reservoir bitumen effect (step 2).

Track 6 is the crossover of $T_{\rm 2LM}$ (T2_LogM) and total porosity (PHIT) logs. In light-fluid-saturated and water-saturated intervals, total porosity and $T_{\rm 2LM}$ should follow the same trend. We plot them on opposite scales to for visual convenience. In zone A of Well 3 (Figure 14), which is a water-saturated interval, two logs clearly

show similar trends. As the porosity increases, the $T_{\rm 2LM}$ increases as well, which shows the dominant effect of pore structure on NMR data. In zones B of both wells, the porosity log shows significant variations whereas the $T_{\rm 2LM}$ log shows a constant low average time. This is an indication of the high-viscosity fluid effect on the NMR response (step 3).

Track 7 presents all the available laboratory and downhole GD measurements. In zone B, the He-injection GD, which is affected by the presence of reservoir bitumen residue, shows a systematically lower GD compared to other measurements such as the XRD calculated (GD_XRD in Well 2) and multimineral analysis (RHOMA_QUA), which are reservoir bitumen independent (step 4).

Track 8 shows thin section analysis (Thin Section) and pressure test results (Good_Press and Failed_Press). In most of the thin sections in zones B, reservoir bitumen has been observed and the pressure test results are "dry." It is an indication of very low fluid mobility either due to low permeability or high fluid viscosity. To differentiate permeability and fluid viscosity effects on the failed pressure tests, we plotted the He-injection

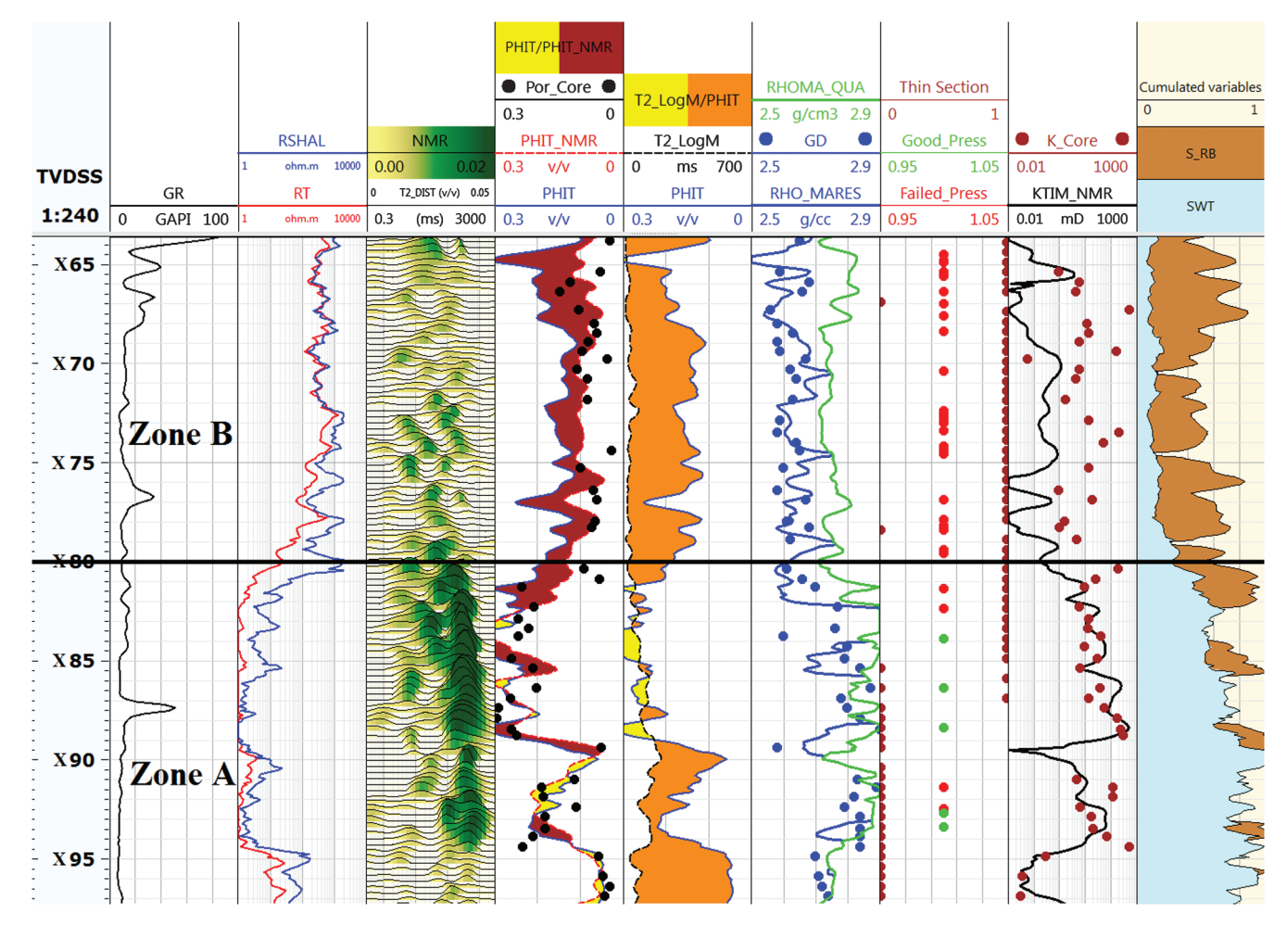


Figure 14. Log and core data for Well 3. Log track details are given in Table 1. The well shows two layers, a water-saturated layer at the top (indicated as zone A) and an oil-saturated interval (indicated as zone B). Quick identification steps are shown in different log tracks. Detailed discussion for each track is given in the "Case study and discussion" section.

Table 1. Log track definitions for Wells 2 and 3 in Figures 13 and 14, respectively.

Track no.	Log and core data
1	True vertical depth sub sea
2	GR
3	Shallow (RSHAL) and deep (RT) resistivity
4	NMR T_2 distribution
5	NMR (PHIT_NMR), and core He-injection (Por_Core) porosity
6	Density porosity (PHIT) and T_2 logarithmic mean (T2_LogM)
7	Effective (RHO_MARES), XRD calculated (GD_XRD) matrix density, He-injection (GD), multimineral model (RHOMA_QUA)
8	Pressure test (good press and failed press) and thin section analysis (thin section)
9	Timur-Coates model NMR (KTIM_NMR) and He-injection (K_Core) permeability
10	Reservoir bitumen (S_SHC) and water saturation (SWT)

permeability results (K_Core) in track 9. The high core permeabilities indicate that the failure in pressure tests is most likely due to the fluid viscosity effect (steps 5 and 6). Note that the permeabilities measured by Heinjection methods are also affected by reservoir bitumen residue and are only indicators of permeability in these intervals.

Ninety-two milliseconds is the common time cut off for capillary bound water volume using NMR log in the Timur-Coates permeability model for carbonate rocks (Coates et al., 1999). In zone B, most of the NMR T_2 distribution (track 4) falls below the cut-off time and results in underestimation of the permeability calculated by the Timur-Coates model (KTIM_NMR in track 9). NMR permeability models are developed assuming T_2 distribution is a representation of pore-size distribution. As mentioned earlier, in reservoir bitumensaturated intervals, the distribution is highly dominated by the short bulk relaxation of the reservoir bitumen.

After identifying the reservoir-bitumen-saturated intervals, the volumetric model presented in this paper was used to calculate the saturation of the reservoir bitumen. The results of the model are shown in track 10. As observed, the saturation of the reservoir bitumen is not constant throughout the wells. The results of the model have been used directly in field-scale reserve calculations.

Conclusions

One of the main challenges in reservoirs with reservoir bitumen is understanding the distribution and the effect that reservoir bitumen has on individual log and core measurements. In this work, thorough petrophysical modeling, using all available data was performed for two wells.

NMR logging is the state-of-the-art method used to differentiate between light and heavy/immobile hydrocarbons. In reservoir-bitumen-saturated intervals, the

NMR T_2 distribution is dominated by the bulk fluid relaxation and is not a representation of the pore-size distribution, so the empirical permeability models using NMR data become unreliable. Heinjection GD from core analysis is underestimated due to the presence of reservoir bitumen residue. Because it is the common source of core-log calibration for density log porosity calculation, using this GD data results in the underestimation of total porosity calculated from the density log. Other sources of porosity such as NMR and He injection also underestimate the total porosity of the rock.

The devised volumetric model is able to explain and quantify the results of the core analysis data when reservoir bitumen is present in the reservoir. The

technique described here can be applied to different reservoirs, regardless of lithology and producing fluid type, for more reliable and precise reservoir evaluation and production planning.

Acknowledgments

The authors would like to thank A. H. Rangwala, V. Mayer, M. K. Borre, and B. Morgan for discussions and comments. Also we would like to acknowledge Maersk Oil Houston, Inc., BP, and Anadarko for permission to publish this work as well as the Organic, Clay, Sand, and Shale Research Center (OCLASSH) at the Colorado School of Mines for their support in finalizing the paper.

References

Akkurt, R., D. Seifert, A. Al-Harbi, T. M. Al-Beaiji, T. Kruspe, H. Thern, and A. Kroken, 2009, Real-time detection of tar in carbonates using LWD triple combo, NMR and formation tester in highly-deviated wells: Petrophysics, 50, 140–152.

Akkurt, R., H. J. Vinegar, P. N. Tutunjian, and A. J. Guillory, 1996, NMR logging of natural gas reservoirs: The Log Analyst, 37, 33–42.

Brownstein, K. R., and C. E. Tarr, 1979, Importance of classical diffusion in NMR studies of water in biological cells: Physical Review A, **19**, 2446–2453, doi: 10.1103/PhysRevA.19.2446.

Carr, H., and E. Purcell, 1954, Effect of diffusion on free precession in nuclear magnetic resonance experiments: Physical Review, **94**, 630–638, doi: 10.1103/PhysRev.94.630.

Chang, D., H. Vinegar, C. Morris, and C. Straley, 1994, Effective porosity, producible fluid and permeability in carbonates from NMR logging: Presented at the SPWLA 35th Annual Logging Symposium.

Coates, G. R., X. Lizhei, and M. G. Prammer, 1999, NMR logging principles and applications: Haliburton Energy Services.

Dumont, H., V. Mishra, J. Y. Zuo, and O. C. Mullins, 2012, Permeable tar mat formation described within context of novel asphaltene science: Presented at the SPE International Petroleum Conference and Exhibition, 163292.

Dunn, K. J., D. J. Bergman, and G. A. Latorraca, 2002, Nuclear magnetic resonance petrophysical and logging applications: Elsevier.

Elseth, T., R. Nicolaysen, and D. E. R. Roberts, 2001, Grain density correction of the density log; a core-log calibration method for improved porosity prediction in mineralized micaceous sandstone reservoirs: Presented at the SPWLA 42nd Annual Symposium.

Freedman, R., C. E. Morriss, C. Straley, M. Johnston, P. N. Tutunjian, and H. J. Vinegar, 1997, Hydrocarbon saturation and viscosity estimation from NMR logging in the Belridge Diatomite: The Log Analyst, **38**, 44–59.

Hirasaki, G. J., S. W. Lo, and Y. Zhang, 2003, NMR properties of petroleum reservoir fluids: Magnetic Resonance Imaging, **21**, 269–277, doi: 10.1016/S0730-725X (03)00135-8.

Jacob, H., 1989, Classification, structure, genesis and practical importance of natural solid oil bitumen ("migrabitumen"): International Journal of Coal Geology, 11, 65–79, doi: 10.1016/0166-5162(89)90113-4.

Larsen, J. W., and K. Kidena, 2002, The sudden release of oil and bitumen from Bakken shale on heating in water: Energy & Fuels, 16, 1004–1005, doi: 10.1021/ef0102465.

LaTorraca, G. A., S. W. Stonard, P. R. Webber, R. M. Carlson, and K. J. Dunn, 1999, Heavy oil viscosity determination using NMR logs: Presented at the SPWLA 40th Annual Logging Symposium, PPP.

Lomando, A. J., 1992, The influence of solid reservoir bitumen on reservoir quality: AAPG Bulletin, **76**, 1137–1152.

Machado, V., P. Frederico, P. Netto, R. Bagueira, A. Boyd, A. Souza, Z. Lukasz, and E. Junk, 2011, Carbonate petrophysics in wells drilled with oil-base mud: Presented at the SPWLA 52nd Annual Logging Symposium, B.

Marschall, D., J. S. Gardner, D. Mardon, and G. R. Coates, 1995, Method for correlating NMR relaxometry and mercury injection data: Presented at the Society of Core Analysis Conference, 9511.

Nascimento, J. D. S., and R. M. R. Gomes, 2004, Tar mats characterization from NMR and conventional logs, case studies in deep water reservoirs, offshore Brazil: Presented at the SPWLA 45th Annual Logging Symposium, FF.

Ruessink, B. H., and D. G. Harville, 1992, Quantitative analysis of bulk mineralogy: The applicability and performance of XRD and FTIR: Presented at the SPE Formation Damage Control Symposium, 23828.

Song, Y. Q., L. Venkataramanan, H. Hürlimann, M. Flaum, P. Frulla, and C. Straley, 2002, T_1 - T_2 correlation spectra obtained using a fast two-dimensional Laplace inversion: Journal of Magnetic Resonance, **154**, 261–268, doi: 10.1006/jmre.2001.2474.

Tissot, B. P., and D. H. Welte, 1984, Petroleum formations and occurrences, 2nd ed.: Springer Verlag.

Wilhelms, A., B. Carpentier, and A. Y. Huc, 1994, New methods to detect tar mats in petroleum reservoirs: Journal of Petroleum Science and Engineering, **12**, 147–155, doi: 10.1016/0920-4105(94)90014-0.



Milad Saidian received a B.S. from the Petroleum University of Technology and an M.S. from Sharif University of Technology. He is a Ph.D. candidate in petroleum engineering at the Colorado School of Mines. His Ph.D. research interests include fluid properties and pore space characterization using NMR for conventional and un-

conventional reservoir rocks, focusing on porosity and pore-size distribution measurement methods. His industrial work experience includes internships at BP America and Maersk Oil Houston, Inc., as a petrophysicist, NIOC as a reservoir engineer, and Maroon Oil and Gas Production Company as a production field engineer.



Torben Rasmussen received M.S.Eng and Ph.D. degrees in physics and materials science from the Technical University of Denmark. He joined Maersk Oil in Copenhagen, Denmark, in 2003 and later worked in Doha, Qatar. Currently, he works as a development petrophysicist with Maersk Oil in Houston, USA. One of Torben's

main interests in petrophysics is understanding the fluid saturation in the reservoir beyond the simplest approaches. Before joining the oil industry, he did postdoctoral work in the field of atomic-scale materials science at the national laboratories in Risø, Denmark, and Los Alamos, New Mexico, USA, and he also worked in the optical fiber industry with a focus on measurements and data analysis.



Mosab Nasser received a B.S. in physics from the Islamic University of Gaza, an M.S. in physics from the International Centre for Theoretical Physics in Italy, and a Ph.D. in physics from the University of Tromso in Norway. He is currently a geophysical advisor at Hess Corporation in Houston, Texas, following five years with

Maersk Oil and eight years with Shell International Exploration and Production in the Netherlands and the USA. He serves as an adjunct professor in the Department of Earth and Atmospheric Sciences at the University of Houston and he is a member of the editorial board of *The Leading Edge* magazine, published monthly by SEG. His research interests include rock physics, AVO, quantitative seismic interpretation, model-based petroelastic seismic inversion, and 4D seismic.



Andres Mantilla received a B.S. in petroleum engineering from the Universidad Industrial de Santander (Colombia), and an M.S. in petroleum engineering and a Ph.D. in geophysics, both from Stanford University. He is currently the director of the Colombian Petroleum Institute, where he leads efforts on applied research

and development for the up-, mid-, and downstream petroleum industry. His technical specializations include rock physics, petrophysics, geologic modeling, reservoir simulation, and economics. He is an earth scientist with 20 years of combined industry experience with Ecopetrol, Maersk Oil, Marathon, and BP, and he specializes in data and discipline integration for reservoir characterization and modeling.



Rick Tobin received a B.S. from James Madison University in 1977, an M.S. (1979), and a Ph.D. (1982) from the University of Cincinnati. He is a geologist specializing in diagenesis and reservoir quality modeling and prediction. He is currently active as a reservoir quality specialist and principal geologist at ConocoPhil-

lips, Houston. He has 32 years of combined industry experience with Amoco, BP, Maersk Oil, and ConocoPhillips. His technical specialties and current research interests include sedimentology, sedimentary petrology, fluid inclusion microthermometry, diagenesis, and reservoir quality modeling.